LA-UR- 10-00324

*Approved for public release; distribution is unlimited.*

| | |
|---|---|
| *Title:* | Macroscopic Crack Formation and Extension in Pristine and Artificially Aged PBX 9501 |
| *Author(s):* | C. Liu, MST-8<br>D.G. Thompson, DE-1<br>LANL |
| *Intended for:* | Proceeding of the 14th International Detonation Symposium<br>Coeur d'Alene, Idaho, USA<br>April 11–16, 2010 |

Los Alamos
NATIONAL LABORATORY
EST. 1943



Form 836 (7/06)

# Macroscopic Crack Formation and Extension in Pristine and Artificially Aged PBX 9501

Cheng Liu[†] and Darla G. Thompson[‡]

[†]Materials Science and Technology Division and [‡]Dynamic and Energetic Materials Division
Los Alamos National Laboratory, Los Alamos, NM 87545

**Abstract.** A technique has been developed to quantitatively describe macroscopic cracks, both their location and extent, in heterogeneous high explosive and mock materials[1]. By combining such a technique with the deformation field measurement using digital image correlation (DIC), we conduct observation and measurement of the initiation, extension, and coalescence of internal cracks in the compression of Brazilian disk made of pristine and artificially aged PBX 9501 high explosives. Our results conclude quantitatively that aged PBX 9501 is not only weaker but also much more brittle than the pristine one, thus is more susceptible to macroscopic cracking.

## Introduction

Cracking is the most dominant mechanical failure mechanism in high explosives (HE) and cracks could affect both safety and performance of weapon and munitions systems. Direct observation and quantitative measurement of the deformation field associated with the formation and extension of one or multiple macroscopic cracks, and quantitative description of the location, extent, and profile of macroscopic cracks are the challenges we have to address to support stockpile stewardship.

When a material is subjected to mechanical loading, macroscopic cracking can start either from the free surface of the specimen, generating the edge cracks, or from the interior of the specimen, forming the internal cracks. In energetic materials, e.g., HEs and solid propellants, it was found that the propensity of generating edge cracks is much higher whenever this is possible. When the possibility of generating surface cracks is completely suppressed, internal cracks will be formed in the interior of the specimen, but the deformation associated with these internal cracks is much more complex. In munitions or weapon systems, free surface in HE may not be the primary concern (since it may not even exist). Thus internal cracking becomes the focus of study concerning fracture and failure in energetic materials.

The Brazilian disk compression provides such a simple test configuration, where only internal cracks can be generated due to the compressive circumferential stress along the free surface. Brazilian disk compression involves a circular disk with a pair of compressive forces acting across its diameter. Such a test configuration was first used as an alternative for measuring elastic constants of materials with very low tensile strength[2] and later it was mainly used for determining the tensile strength of brittle materials, e.g., concretes and rocks[3, 4]. It has also been used in studying microcracking of the PBX 9501 high explosive[5, 6]. To directly observe the evolution of the deformation field, we use the optical technique of

digital image correlation (DIC)[7]. The technique of combining the Brazilian disk and the DIC has been applied to polymer epoxy resin[8] and PBX 9501[9].

The objective of our investigation is to observe and to quantify processes of macroscopic crack initiation and extension in both the pristine and artificially aged PBX 9501 high explosives and at three different temperatures, −15°C, 23°C, and 50°C. The quantitative comparison will be conducted from three aspects: (1) the overall response of the disk specimen at different temperatures, (2) the evolution of macroscopic crack opening displacement at several vertical locations of each specimen based on the displacement field measurement of DIC, and (3) the formation and extension of localized cracked region of each specimen based on a technique developed recently[1].

## Material and measuring technique

PBX 9501 is a heterogeneous composite with 5 wt% polymeric binder and 95 wt% HMX (cyclotetramethylene tetranitramine) crystals in a bimodal size distribution. The polymeric binder is comprised of 50 wt% Estane, a polyurethane polyester, and 50 wt% nitroplasticizer (NP), which is a eutectic mixture of bis (2,2-dinitropropyl) formal and bis (2,2-dinitropropyl) acetal. Typically, the HMX powders are mixed with three parts of coarse crystals with average crystal size of 250 $\mu$m and with one part of fine crystals with average crystal size of 8 $\mu$m. The volume fractions of the coarse and fine HMX particles are 69.5 vol% and 23.2 vol%, respectively. After combining with the polymer binder, the mixture is then hydrostatically pressed into an explosive compound.

To obtain artificially aged PBX 9501, we use the stockpile-returned HE charges and subject them through an accelerated aging process. The HE parts were suspended on wire mesh shelves inside a gastight cylindrical container, so that the parts can expose to the atmosphere within the container. A saturated Na-Cl solution was placed on the bottom of the container, and the entire assembly was heated to and maintained at 70°C temperature and at 75% relative humidity for the duration of each cylinder's aging time. The interior walls of the cylindrical container were painted with the nitroplasticizer (NP) to mitigate the NP loss of HE during aging. At the end of the process, the molecular weight (MW) of the estane binder was reduced from the nominal 80–100 kD to about 14.9 kD.

In this investigation, we use the digital image correlation (DIC) technique to obtain deformation field on the specimen surface. This technique relies on the computer vision approach to extract the whole-field displacement data, that is, by comparing the features in a pair of digital images of the specimen surface before and after deformation. Detailed description of underlying principles of the DIC technique can be found in literature[7].

## Overall response and deformation observations

The Brazilian disk specimen we used in this study has the nominal dimension of 25.4 mm in diameter and 6.35 mm in thickness. We also used a loading fixture with circular anvil for applying compressive load to the specimen. The radii ratio of the circular anvil and the circular disk is 1.25:1. The schematic of the loading fixture and the disk specimen is shown in Fig. 1(a). On the surface of the disk specimen, a

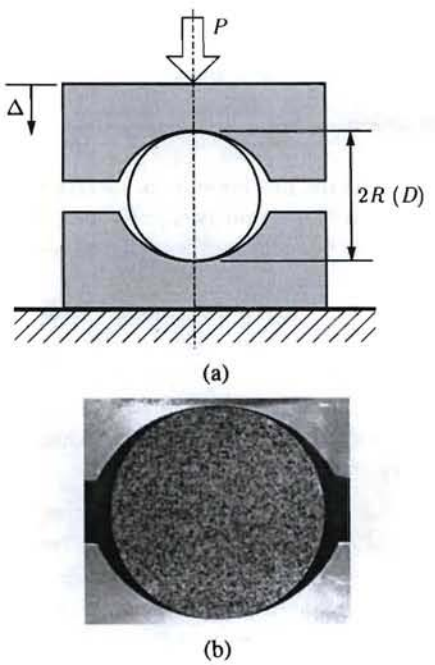


Fig. 1. (a) Schematic of the loading fixture and disk specimen; (b) Random speckle image of the disk specimen.

random speckle pattern was painted by spraying a black paint, as shown in Fig. 1(b).

We used a conventional Instron 5567 screw-driven loading frame, with the MTS ReNew/E System controller, to load the specimen at a constant crosshead moving velocity. We chose the crosshead moving velocity to be 0.5 mm/minute. An environmental chamber was used to control the testing temperature. After the disk specimen was placed in the fixture, the door of the environmental chamber was closed. The temperature was then raised or lowed to the preset temperature at the rate of 1°C/minute. When the desired temperature was reached, we waited for 15 minutes so that the specimen can reach thermal equilibrium.

During the test, the applied load and the crosshead displacement were monitored and recorded at the sampling rate of 15 Hz. A CCD camera, with the resolution of 1628 × 1236 pixels, was setup in front of the window of the environmental chamber. A series of images was captured during the test at the framing rate of 5 frames/second. The random speckle image has a spatial resolution of about 23 $\mu$m/pixel. Before each test, a small pre-load ($\sim$ 1 N) was applied to keep the disk specimen in place.

Figure 2 presents the variation of applied compressive load as a function of the change of specimen diameter for all the tests of PBX 9501 Brazilian disks, where 9 pristine and 12 aged specimens are included. In Fig. 2, the applied compressive force $P$ was normalized by the product of the initial thickness $W$ and the initial radius $R$ of the disk specimen, and the diameter change $\Delta$ was normalized by the initial specimen diameter $D$. The variation of applied load as a function of deformation, as shown in Fig. 2, resembles the common behavior of the heterogeneous high explosive PBX 9501 and its various simulant mocks. As the deformation increases, the applied load first monotonically increases, and then turns around and gracefully decreases. The peak load is believed to be associated with localized deformation occurring within the specimen. The maximum load is strongly dependent on temperature.

We choose the maximum load (strength) and the total deformation at maximum load as the global parameters associated with the specimen failure. The variations of these characterizing parameters as function of temperature are shown in Fig. 3. For pristine PBX 9501, the total deformation at failure is insensitive of temperature, while the strength monotonically decreases as temperature becomes higher. For aged PBX 9501, both the total deformation at failure and sample strength monotonically decreases as temperature rises. Figure 3 also shows the amount of reduction of both the strength and the total deformation at failure from pristine to aged PBX 9501. Since the amount of load that the aged PBX 9501 specimen can carry at failure and the amount of deformation that the aged PBX 9501 specimen can sustain are significantly reduced, the aged PBX 9501 with lower molecular weight is much weaker and more brittle. Such reduction in strength and increasing in brittleness are even more profound at higher temperatures.

Digital image correlation (DIC) calculation was carried out on the series of random speckle images to determine the displacement field during the deformation of the disk specimens. Assuming the local deformation is homogeneous, the deformation gradient and the rigid translation of a small region (or subcell) are sought by minimizing the so-called correlation function. From this the displacement at the center of the subcell is determined. The subcell size used in the DIC calculation is 31 pixel, or approximately 0.8 mm. Each image was compared against the initial image, where no deformation has occurred, and displacement field over the entire disk surface at each moment of time was obtained.

We select four different moments of time during the deformation process of a pristine and an aged PBX 9501 disk specimen tested at 23°C and present the contour plots of the displacement component ($u$ in the horizontal direction) and the strain component (normal strain $\epsilon_x$ in the horizontal direction) in Fig. 4. Moment A is when the applied compressive load has not reached the maximum value. Moment B corresponds to the moment when compressive load is at the maximum. Moment C is on the way when the applied compressive load decreases while the overall deformation is still increasing. Finally, moment D is when the applied compressive load reaches its local minimum and is about to slowly increase again (see Fig. 2).

For pristine PBX 9501 (Fig. 4(a)), at the moment A, the measured displacement field resembles the characteristics of those obtained from the elastic

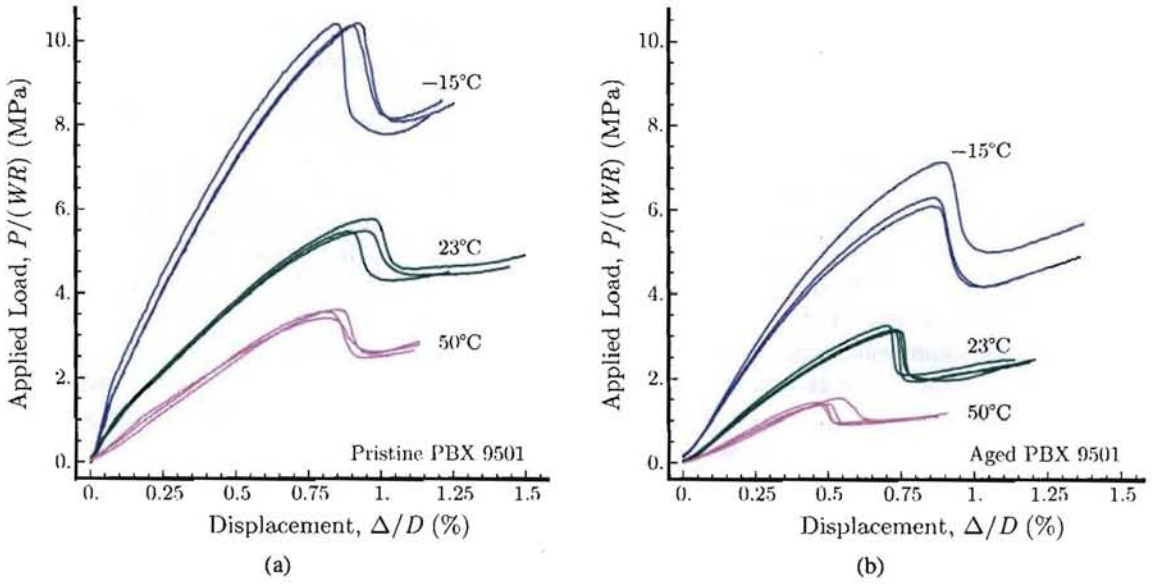


Fig. 2. Variation of applied compressive load $P$ as function of sample diameter change $\Delta$ for different temperatures: (a) pristine and (b) artificially aged PBX 9501.

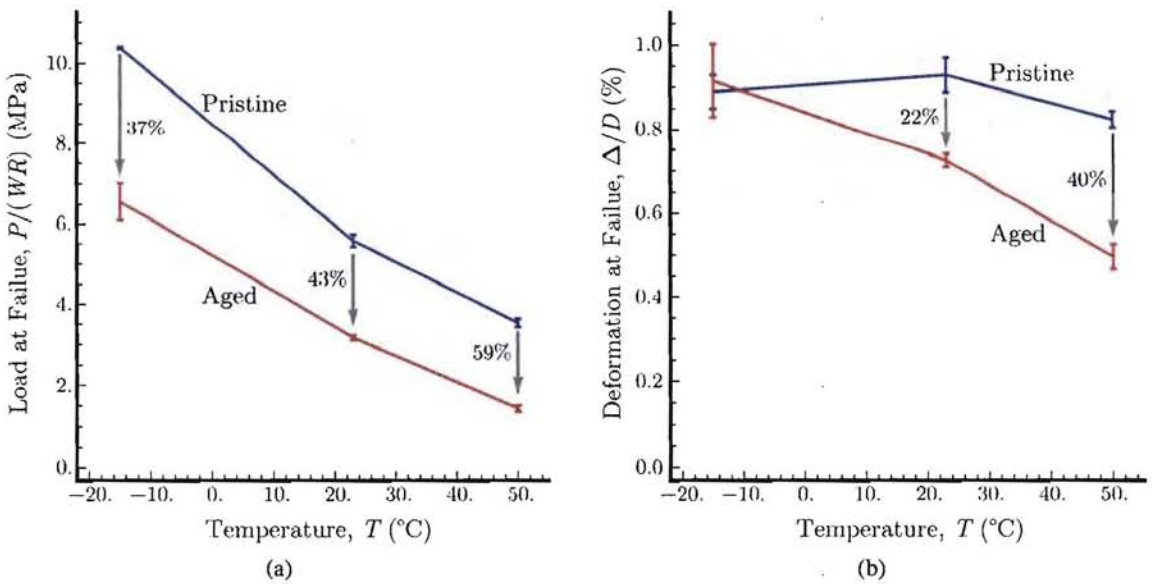


Fig. 3. (a) Reduction of maximum load (strength) and (b) reduction of total deformation at maximum load as function of temperature.

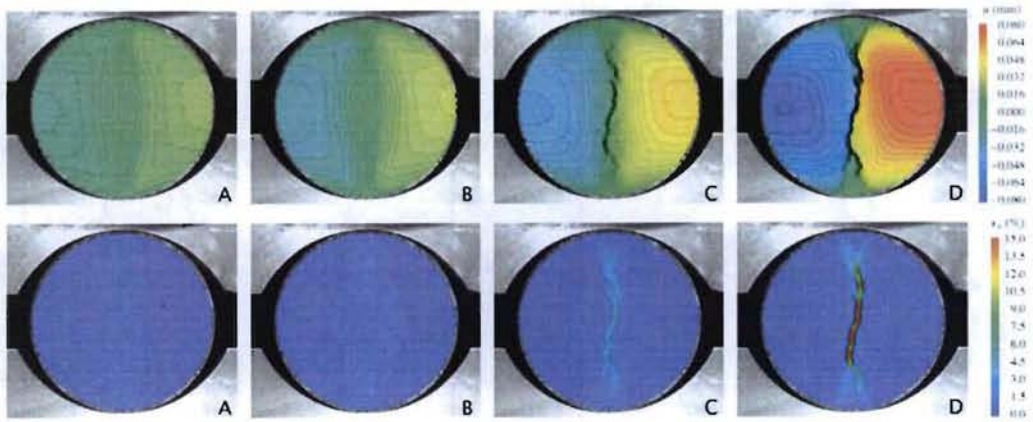


(a)

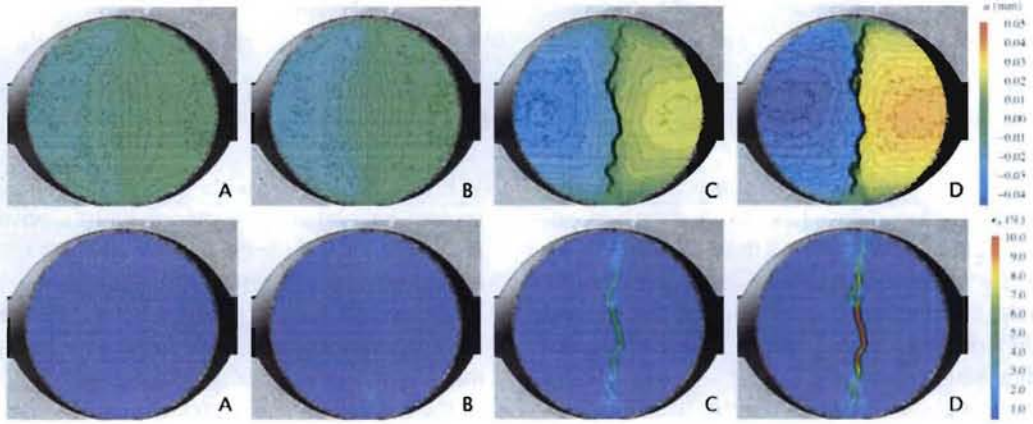


(b)

Fig. 4. Selected contour plots of $u$ and $\epsilon_x$-field of (a) a pristine and (b) an aged PBX 9501 disk tested at 23°C.

solution[8]. However, the strain component $\epsilon_x$ at this moment indicates higher deformation regions near the two loading boundaries. At moment B, where compressive load is at the maximum, the measured displacement field is still similar to those given by the elastic solution, but the concentration of the gradient of the displacement component $u$ has become apparent from both the contour plot of $u$-field and of the $\epsilon_x$-field. In fact, $\epsilon_x$-field contour plot at moment B has shown multiple sites where strain localization has occurred. From the contour plots at moment C, one observes that the localized deformations became more profound and they have extended and propagated toward the center of the disk specimen, and finally coalesced in the center region. At moment D, the localized deformation has fully developed and as the overall deformation proceeded further, the extent of the localized deformation will not change much, only its magnitude, as signified by the strain component $\epsilon_x$, will increase. Similar characteristics is observed for the aged PBX 9501 as well, see Fig. 4(b). In fact, the deformation sequence is similar in both pristine and aged PBX 9501 disk specimens and at all test temperatures, although details may vary from specimen to specimen due to the heterogeneous nature of material's microstructure.

**Macroscopic crack opening evolution**

Measurement of the displacement field on the surface of the disk specimen has indicated that for any given horizontal line, prior to the maximum load, the displacement profile is continuous suggesting

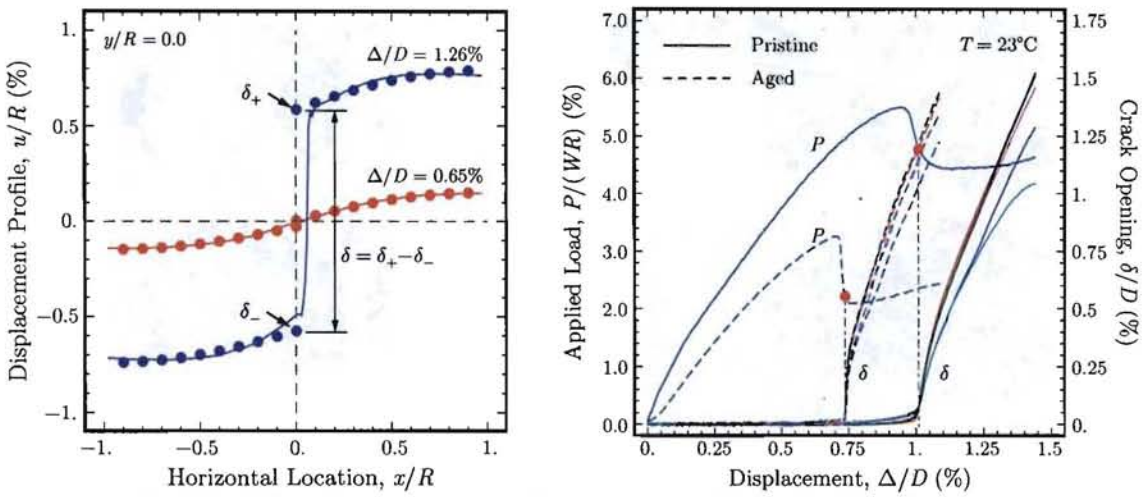


Fig. 5. (a) Determination of crack opening at a given vertical location. (b) Comparison of crack opening evolution of pristine (solid lines) and aged (dashed lines) PBX 9501 tested at 23°C.

continuous deformation. After the peak load, discontinuous displacement starts to develop indicating macroscopic cracking (e.g., the $u$-field in Fig. 4). Meanwhile, measurement also indicates that after the peak load, the displacement profiles on the left and the right side of the discontinuity (or crack) along a horizontal line remain self-similar. As a result, we may use the elastic solution for the Brazilian disk without cracking[8] combined with the measurement of displacement profile to determine quantitatively the crack-opening displacement at any vertical location of the disk specimen.

Figure 5(a) shows schematically the scheme of determining the crack opening displacement $\delta$ at a given vertical location, in this case $y = 0$. Away from the vertical center region, the displacement profile $u$ after the formation of discontinuity remains self-similar. This can be seen in Fig. 5(a) that away from vertical diameter $x = 0$ the solid curves at $\Delta/D = 1.26\%$ have the same shape as the curves at $\Delta/D = 0.65\%$, where onset of discontinuous displacement is about to start. The elastic expression[8] for $u$, which carries undetermined parameter $\delta_+$ or $\delta_-$ is fit to the solid curve. The intersections of the fitted curves (the solid symbols) with the vertical diameter ($x = 0$) determine the parameters $\delta_\pm$, and the crack opening displacement at the given vertical location is calculated as $\delta = \delta_+ - \delta_-$.

Figure 5(b) presents the evolution of the macroscopic crack opening displacement of a pristine and an aged PBX 9501 specimen tested at 23°C. Different colors represent different locations along the vertical diameter. In both cases, substantial crack opening occurs after the applied compressive load reaches maximum, further confirm that the softening portion of the loading curve is associated with macroscopic damage and fracture. For pristine PBX 9501 such a transition occurs at about $\Delta/D = 1\%$, prior to which one observes some slow increase of crack opening as defined by the procedure shown in Fig. 5(a). Based on further analysis, which will be discussed later, this slow increase represents precursor of macroscopic cracking, such as the accumulation of localized damage. In fact, these slow occurring events happen in regions close to the top and the bottom loading surfaces, contradicting the belief that macroscopic crack starts at the center of the disk specimen, which is the case for true brittle solids. The transition in aged PBX 9501 occurs at about $\Delta/D = 0.75\%$ in a more drastic fashion. It seems that the macroscopic crack initiation at all vertical locations along the diameter takes place almost simultaneously. The rate at which the crack opens up, represented by the slope of the curves in Fig. 5(b), is much faster in the aged PBX 9501 sample, since the crack opening curves are much steeper for aged PBX 9501 than that for

pristine PBX 9501. Similar observations are made for specimens tested at other temperatures. Analysis of the evolution of crack opening, once again, concludes that the aged PBX 9501 with lower molecular weight is more brittle, and this conclusion is based on observations of local cracking behavior.

**Cracked region formation and extension**

One of the major challenges in studying fracture and failure of high explosives and their mock materials, is that it is very difficult to actually see the cracks before they grow large enough. This is mainly because that the material is highly heterogeneous with a very complicated microstructure and the contrast of the mechanical properties of the constituents is also remarkably high. Even though the results shown in Fig. 4 clearly suggest the presence of macroscopic cracks in the disk sample and the analysis presented in Fig. 5 can provide quantitative description regarding crack opening, we are still unable to pinpoint the exact moment of crack initiation, the exact location of the macroscopic crack tip, and the exact extent of the region occupied by cracks.

A technique has been developed recently to quantitatively describe macroscopic cracks, both their location and extent, in heterogeneous high explosive and mock material[1]. This approach is based on some quantitative information that has been generated during the DIC calculations of the deformation field. DIC depends on the computer vision approach by comparing features in a pair of digital images of a specimen surface, before and after deformation, to identify the displacement at a given data point. The primary assumption that the DIC makes is that the essential characteristics of the speckle pattern remains the same before and after the deformation. The only changes that a small region of the speckle pattern can experience, are translation, stretches in different directions, and shear. To determine the distortion of the small region, DIC uses the correlation coefficient, designated as $c$, as a discriminating parameter. The correlation coefficient is a function of the two random speckle images before and after deformation, and it also depends on the aforementioned changes of the small region. When the distortion of the small region is such that the features of the two random speckle images match each other, the correlation coefficient reaches a minimum. Ideally, if the above-mentioned assumptions are truly held, the perfect match of the two speckle images implies that the correlation coefficient $c = 0$. In reality, however, especially for the heterogeneous material we are dealing with, the correlation coefficient does not converge to zero but to a small positive number.

When damage or cracks develop in the small region during deformation, the fundamental assumption that DIC makes in order to determine the deformation of that region, no longer holds true. However, the numerical scheme in DIC calculation is more tolerable and the correlation coefficient may still be able to attain minimum. But the absolute value of this minimized correlation coefficient becomes much larger than the one when no damage or cracks are present in the region. Meanwhile, as the cracking in a small region becomes more severe, the increase of the minimized correlation coefficient also becomes more significant. Usually, in DIC calculation, the correlation coefficient is only used for judging the numerical convergence and we are not concerned about the magnitude of the correlation coefficient itself. But based on the above discussion, one may use the distribution of the minimized correlation coefficient at each location to reveal and quantify the location and extent of cracks in a test specimen.

Note that the correlation coefficient $c$ is a scalar field, as shown in Fig. 6, and will evolve as a function of time during the deformation.

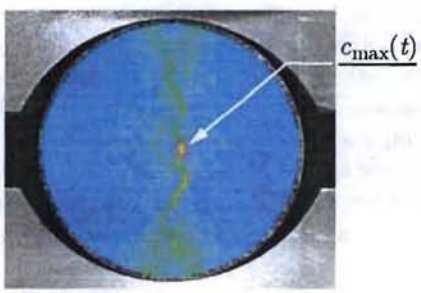


Fig. 6. Schematic of identifying parameter $c_{\max}$ for a given moment of time.

For simplicity, at any given moment of time, we only select the maximum $c$ in the entire field at that moment and designate it as $c_{\max}(t)$, as shown in Fig. 6. We will monitor the variation of $c_{\max}(t)$ as the deformation proceeds. We also normalize $c_{\max}(t)$

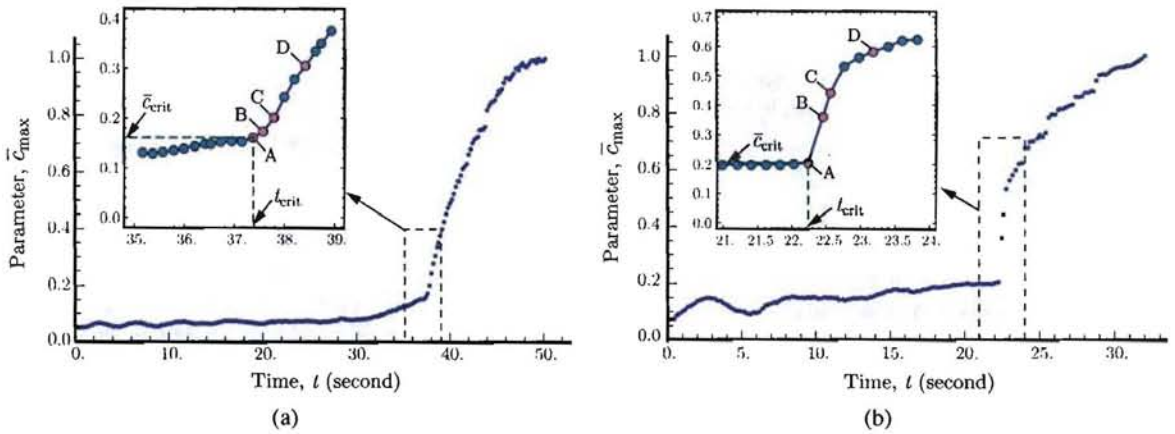


Fig. 7. Evolution of the normalized correlation parameter $\bar{c}_{max}$ as function of time for (a) a pristine and (b) an aged PBX 9501 specimens tested at 23°C.

such that during the entire deformation process of the test, the normalized correlation coefficient varies between 0 and 1.

Figure 7 presents the variation of the normalized correlation coefficient $\bar{c}_{max}$ as a function of time for a pristine and an aged PBX 9501 disks tested at 23°C. A striking feature of such a variation is that parameter $\bar{c}_{max}$ exhibits a sharp transition during the process of deformation. Take the pristine PBX 9501 (Fig. 7(a)), during the early stage of the deformation, parameter $\bar{c}_{max} < 0.16$ consistently and changes very little. After a particular moment of time, parameter $\bar{c}_{max}$ monotonically increases drastically until the late stage of deformation, where parameter $\bar{c}_{max}$ stays closer to 1.0. The transition from slow variation to the monotonic ascent is so sudden and distinctive, where the insert in Fig. 7(a) provides more detailed depiction of such a transition. The fast paced ascent of parameter $\bar{c}_{max}$ indicates that after that particular moment of time, correlation of portion of the speckle images has degraded and the degree of such correlation degradation becomes ever severe as the overall deformation proceeds further. Since during the deformation process, which lasts less than 1 minute, all testing conditions remain unchanged, the only attributing reason for the correlation degradation is the variation of the character of the portion of the speckle image changes. At the same time, the optical system during the same period of time experiences no change as well, for example the lighting condition, the variation of the character of the speckle pattern is solely due to the change of material beneath it, and in case, it is the damage and cracking of the sample.

Two parameters can be easily identified from this transition. One is the critical time $t_{crit}$, at which the transition occurs. The other is the value of the normalized correlation coefficient, denoted as $\bar{c}_{crit}$, which represents a threshold such that when $t < t_{crit}$ the normalized correlation coefficient at any location of the sample surface is always less than $\bar{c}_{crit}$, while for $t > t_{crit}$, the maximum normalized correlation coefficient at that moment is never less than $\bar{c}_{crit}$. The same observation and conclusion hold true for the aged PBX 9501 as well, as shown in Fig. 7(b).

The critical instant of time $t_{crit}$, designated as moment A in the inserts of Fig. 7, identifies unambiguously the exact moment of macroscopic crack initiation in the Brazilian disk specimen, which has been an unresolved issue for investigating crack and damage initiation in energetic materials. Such a critical moment $t_{crit}$, when transferred to the overall response of the disk specimens and the evolution of local crack opening, is indicated by the solid dots and the vertical dotted-dashed lines in Fig. 5(b). For the aged PBX 9501, the critical moment $t_{crit}$ corresponds exactly to the dramatic crack opening as shown in Fig. 5(b). However, for the pristine PBX 9501, we saw that localized damage develops prior to the formation of macroscopic cracks.

The second critical parameter, $\bar{c}_{crit}$, can be used to quantify the location and extent of the cracked regions in the disk specimen. Figure 8 presents the

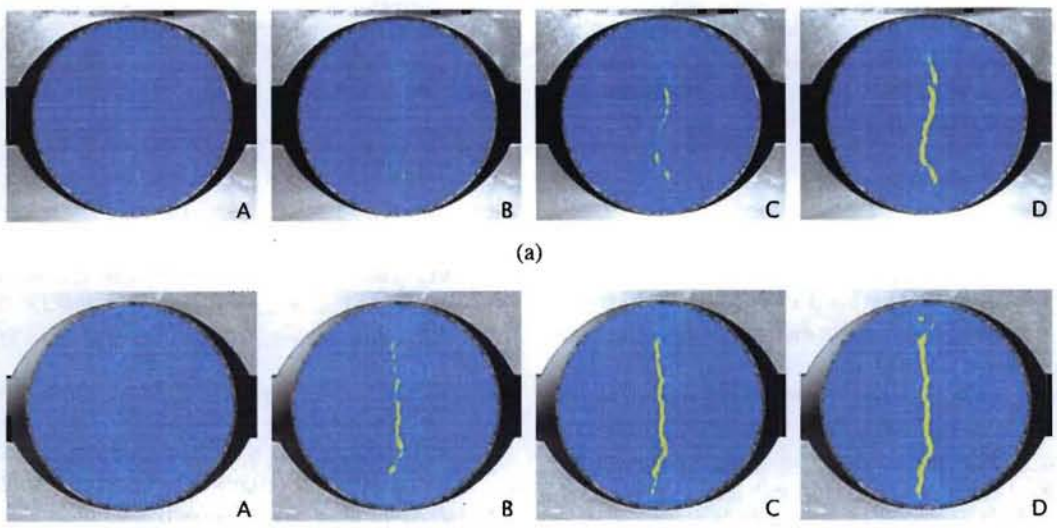


Fig. 8. Selected contour plots of normalized correlation coefficient of (a) a pristine and (b) an aged PBX 9501 disk tested at 23°C. The cracked regions are highlighted by the color yellow.

evolution of the cracked regions in both the pristine and the aged PBX 9501 disk specimens. The selected moments, A, B, C, and D, have been indicated in the inserts of Fig. 7. The contour plots in Fig. 8 represent the normalized correlation coefficient field, so that the critical parameter $\overline{c}_{crit}$ is just one of those contours. At the instant of $t_{crit}$ (moment A in both Figs. 8(a) and 8(b)), the normalized correlation coefficient over the entire sample surface is no larger than $\overline{c}_{crit}$ (e.g., see Fig. 7). In the subsequent moments, B, C, and D, in some regions within the sample surface the normalized correlation coefficient exceeds the critical parameter $\overline{c}_{crit}$. These regions are highlighted in yellow in Fig. 8, and the parameter $\overline{c}_{crit}$ itself represents the boundaries of those yellow regions. As we have discussed before, the normalized correlation coefficient when exceeds the critical parameter $\overline{c}_{crit}$, indicates the degradation of the speckle image, which is caused by the alternation of the material underneath the image. Therefore, those yellow regions are the ones occupied by macroscopic cracks.

For pristine PBX 9501 (Fig. 8(a)) and at the moment B, there is only one single small region, about a quarter of the disk diameter from the bottom loading surface, where cracking has been initiated. At the next moment C, the small cracked region formed at moment B grows larger,but at the same time, there are several disconnected new cracked sites formed. At moment D, those disconnected cracked regions enlarge and coalesce. By the end of the test, a single dominant crack is generated along the center section of the disk specimen. For aged PBX 9501 (Fig. 8(b)), multiple cracking sites along the center section of the disk specimen have been formed and by the moment C, those cracked region already connect together and form a single large dominant crack.

Note that from moment A to B and from moment B to C, the time increments are 0.2 second in both the pristine and the aged PBX 9501, while from moment C to D, it is 0.6 second. The sequence of macroscopic crack formation, extension, and coalescence is quite different in pristine PBX 9501 from that in aged PBX 9501. In pristine PBX 9501, such a process is more gradual and relatively slow. Meanwhile, prior to the formation of macroscopic cracks, there is localized damage accumulation in pristine PBX 9501. Whereas in aged PBX 9501 the process is much faster and the formation of macroscopic cracks is more sudden, further confirm the observations in Fig. 5(b). If we characterize the failure process in pristine PBX 9501 as the one associated with a quasi-brittle material, the failure process in aged PBX 9501 does indeed possess the character of a true

brittle solid. Although, we only looked at the situations that the PBX 9501 specimens tested at ambient temperature (23°C), similar findings are made at other temperatures as well.

## Concluding remarks

In this investigation, we studied the process of the formation and extension of internal cracks in both pristine and artificially aged PBX 9501 high explosives, subject to quasi-static mechanical loading condition and at three different temperatures. The characteristic factor that differentiating pristine and aged PBX 9501, is the molecular weight of the polymeric binder, which has been reduced from the nominal 80–100 kD to about 15 kD through the aging process.

We combined the Brazilian disk compression testing configuration, the optical digital image correlation (DIC) technique, and an analysis scheme for revealing and quantifying macroscopic cracks in heterogeneous solid. We were able to correlate the overall specimen response with the localized damaging and cracking behavior. The effect of aging does affect the stiffness and the strength of the material. In the aspect of mechanical failure, aging makes the PBX 9501 appear more brittle. The observations and measurements presented in this study at local scale, provide quantitative results describing the entire failure process, and may shed light on the underlying mechanisms.

The experimental results will be combined with detailed numerical simulations for supporting model development and model verification and validation. The technique developed in this investigation can also be extended to analyze scenarios relevant to other high explosive applications, like foreign object damage and/or near-by blast effects.

## Acknowledgments

Los Alamos National Laboratory is operated by Los Alamos National Security (LANS), LLC for the Department of Energy (DOE) and the National Nuclear Security Administration (NNSA). This study was supported by the Joint DoD/DOE Munitions Program (JMP), the W88 program, and the Enhanced Surveillance Campaign (ESC). The authors would also like to thank Mr. M.L. Lovato and Ms. R. DeLuca of Los Alamos National Laboratory for the assistance in conducting the experiments presented in this study.

## References

1. Liu, C., Cady, C. M., Lovato, M. L., and Rae, P. J., A technique for revealing and quantifying cracks in heterogeneous solids, Los Alamos National Laboratory Report, LA-UR-09-02906, 2009. Submitted for publication in *Exp. Mech.*

2. Hondros, G., The evaluation of Poisson's ratio and the modulus of materials of a low tensile resistance by the Brazilian (indirect tensile) test with particular reference to concrete, *Australian J. Appl. Sci.*, 10:243–268, 1959.

3. Mellor, M. and Hawkes, I., Measurement of tensile strength by diametral compression of discs and annuli, *Eng. Geo.*, 5:173–225, 1971.

4. Hudson, J. A., Brown, E. T., and Rummel, F., The controlled failure of rock discs and rings loaded in diametral compression, *Int. J. Rock Mech. Mining Tech.*, 9:241–248, 1972.

5. Rae, P. J., Goldrein, H. T., Palmer, S. J. P., Field, J. E., and Lewis, A. L., Quasi-static studies of the deformation and failure of $\beta$-HMX based polymer bonded explosives, *Proc. Royal Soc. London A*, 458:473–462, 2002.

6. Rae, P. J., Palmer, S. J. P., Goldrein, H. T., Field, J. E., and Lewis, A. L., Quasi-static studies of the deformation and failure of PBX 9501, *Proc. Royal Soc. London A*, 458:2227–2242, 2002.

7. Sutton, M. A., McNeill, S. R., Helm, J. D., and Chao, Y. J., Advances in two-dimensional and three-dimensional computer vision. *Topics Appl. Phys.*, 77:323–372, 2000.

8. Liu, C., Elastic constants determination and deformation observation using Brazilian disk geometry, *Exp. Mech.*, DOI 10.1007/s11340-009-9281-2, 2010.

9. Liu, C. and Thompson, D. G., Deformation and failure of PBX 9501 high explosive, Los Alamos National Laboratory Report, LA-UR-08-0275, 2008.